




Sarcopenia in a mice model of chronic liver disease: role of the ubiquitin–proteasome system and oxidative stress

Fabián Campos^{1,2} · Johanna Abrigo^{1,2} · Francisco Aguirre^{1,2} · Bruno Garcés^{1,2} · Marco Arrese³ · Saul Karpen⁴ · Daniel Cabrera^{3,5} · Marcelo E. Andía^{6,7} · Felipe Simon^{1,2} · Claudio Cabello-Verrugio^{1,2} 

Received: 13 December 2017 / Revised: 6 June 2018 / Accepted: 11 June 2018 / Published online: 20 June 2018
© Springer-Verlag GmbH Germany, part of Springer Nature 2018

Abstract

Sarcopenia is the loss of muscle mass and strength produced by aging or secondary to chronic diseases such as chronic liver disease (CLD). Although not all types of sarcopenia involve the same features, the most common are decreased fiber diameter and myosin heavy chain (MHC) levels, increased activity of ubiquitin–proteasome system (UPS) and reactive oxygen species (ROS). In this study, we aim to characterize the development of sarcopenia secondary to CLD induced by the hepatotoxin 5-diethoxycarbonyl-1,4-dihydrocollidine (DDC). For this purpose, four-months-old male C57BL6 mice were fed with normal diet or DDC supplemented diet for 6 weeks. Functional tests to evaluate muscle strength, mobility, and motor skills were performed in alive mice. The muscle strength in isolated gastrocnemius was also assayed via electrophysiological measurements. Morphometric measures of fibers' diameter, total and ubiquitinated protein levels of myosin heavy chain (MHC), E3 ubiquitin ligases, ROS, and oxidation-dependent modified proteins in gastrocnemius tissue were also determined. Our results demonstrated that mice fed the DDC diet developed muscle wasting as evidenced by a loss of muscle mass and decreased muscle strength. The muscles of mice fed with DDC diet have a decreased diameter of fibers and MHC levels, also as increased MuRF-1 and atrogin-1 protein levels, ROS levels, and oxidation-modified protein levels. Additionally, control and DDC mice have the same food and water intake as well as mobility. Our results demonstrate mice with CLD develop sarcopenia involving decreased levels of myofibrillar proteins, increased UPS, and oxidative stress, but not for impaired caloric intake or immobility.

Keywords Sarcopenia · Chronic liver diseases · Hepatotoxin · UPS · Oxidative stress

F.C. and J.A. contributed equally to the present work.

Electronic supplementary material The online version of this article (<https://doi.org/10.1007/s00424-018-2167-3>) contains supplementary material, which is available to authorized users.

✉ Claudio Cabello-Verrugio
claudio.cabello@unab.cl

¹ Laboratorio de Patologías Musculares, Fragilidad y Envejecimiento, Departamento de Ciencias Biológicas, Facultad de Ciencias de la Vida, Universidad Andres Bello, Avenida República 239, 8370146 Santiago, Chile

² Millennium Institute on Immunology and Immunotherapy, Santiago, Chile

³ Departamento de Gastroenterología, Facultad de Medicina, Pontificia Universidad Católica de Chile, Santiago, Chile

⁴ Department of Pediatrics, Emory University School of Medicine, Atlanta, GA, USA

⁵ Facultad de Salud, Departamento de Ciencias Químicas y Biológicas, Universidad Bernardo O Higgins, Santiago, Chile

⁶ Biomedical Imaging Center, Pontificia Universidad Católica de Chile, Santiago, Chile

⁷ Radiology Department, School of Medicine, Pontificia Universidad Católica de Chile, Santiago, Chile

Introduction

Skeletal muscle is one of the most abundant tissues in the body and makes the generation of force, movement, and breathing possible. Since skeletal muscle is exposed to many different internal and external stimuli, it has high plasticity, evidenced by changes in muscle mass. Skeletal muscle atrophy can be defined as the loss of muscle mass with a concomitant decrease in function and force generation [12]. Among the main factors altering muscle mass are aging, disuse, and several chronic diseases such as cancer, cardiac, renal, and liver pathologies. Sarcopenia is defined as a complex syndrome characterized by loss of body weight, muscle mass, and strength which is not only developed during aging but also by chronic illness or inflammatory conditions [29]. During sarcopenia, the major degraded skeletal muscle proteins are myofibrillar proteins such as myosin heavy chain (MHC) which is a key component in the process of muscle contraction [14, 37]. One of the main mechanisms involved in this catabolic process is the ubiquitin–proteasome system (UPS) [10, 67]. Overactivation of the UPS during muscle wasting is characterized by a muscle-specific increase of type E3 ubiquitin ligases, atrogen-1 (Muscle Atrophy F-box, MAFbx), and MuRF-1 (Muscle-specific RING-finger protein 1) [67]. Oxidative stress is also present in skeletal muscle wasting [63, 69]. The main oxidant types are reactive oxygen species (ROS). Oxidative stress has been functionally linked to muscle wasting through UPS activation, where increased ROS activates proteasome-dependent protein degradation through the expression of atrogen-1 and MuRF-1 [1, 63, 66]. Another consequence of oxidative stress is oxidative injury generated in the cell, as evidenced by protein and lipid oxidation [5, 62, 68].

Among the causes of muscle wasting are chronic liver diseases (CLD) [16, 40]. CLDs are a group of liver dysfunctions resulting in severe injury characterized by hepatocellular alterations and fibrosis, which progress to cirrhosis [8]. Several types of liver damage are classified as CLDs, including fibrosing cholangiopathies, a group of cholestatic liver diseases affecting biliary ducts responsible for transporting and modifying bile [44]. Xenobiotic-induced cholangiopathies produce biliary disease that may progress to vanishing bile duct syndrome, biliary fibrosis, and cirrhosis [46]. CLD results in cirrhosis and, usually, in end-stage liver disease requiring a liver transplant to extend survival [78]. None of these consequences is reversible [8]. There are few effective therapeutic options for treating CLD etiology, the consequence of which is an increased incidence of cirrhosis [22, 36]. The most recognized clinical complications of CLD include ascites, encephalopathy, portal hypertension, renal dysfunction, hepatocellular carcinoma, and malnutrition [6, 8, 28]. However, and despite being less studied, sarcopenia is the most common complication and adversely affects survival, quality of life,

and outcomes after liver transplantation, as well as being responsible for the development of additional health complications [22, 34, 52, 71]. The few, but highly relevant, studies relating CLD and sarcopenia confirm the negative impacts of sarcopenia. One of these studies found sarcopenia is an independent predictor of mortality in cirrhosis patients [52]. Moreover, a retrospective analysis in CLD patients found the loss of muscle mass to be an independent predictor of mortality for patients awaiting liver transplantation [22, 74]. Thus, sarcopenia associated with CLD is gaining relevance in hepatology, with clinicians trying to incorporate this condition as a new parameter for consideration in liver transplants [21, 22]. However, the mechanisms underlying sarcopenia in CLD are not yet fully understood. In this study, we evaluated the mechanism involved in muscle weakness in CLD, using a previously characterized murine model of xenobiotic-induced cholangiopathy that produces hepatobiliary injury and biliary fibrosis by intake of the hepatotoxin 3,5-diethoxycarbonyl-1,4-dihydrocollidine (DDC) [32].

Our results indicate mice fed a DDC supplemented diet for 6 weeks developed muscle wasting, evidenced by loss of muscle mass and decreased muscle strength. Muscles of these sarcopenic mice have a decreased diameter of muscle fibers, reduced MHC, and increased UPS components and ROS levels. Furthermore, mice fed either normal or DDC diet have the same food and water intake as well as motor skills and mobility.

Our data showed mice with CLD induced by a hepatotoxin develop sarcopenia which involves decreased levels of myofibrillar proteins, increased UPS activity, and oxidative stress. Notably, we also demonstrated muscle weakness is not produced by differential caloric intake or immobility.

Methods

Animals Male C57BL/6J (16 weeks old) strain of mice was used. The animals were randomized and separated into experimental groups, and three independent experiments were performed. Two experimental groups (five to seven animals/group) were designed: normal diet (Control) and diet supplemented with 0.1% (1 mg/kg) of 5-diethoxycarbonyl-1,4-dihydrocollidine (DDC) [32]. The mice were fed with Control or DDC diet for 6 weeks. At the end of the experiment, the animals were euthanized under anesthesia and the gastrocnemius (GA) muscles were dissected, removed, separated from plantaris, weighed and rapidly frozen, and stored at -80°C until processing. All applicable international, national, and/or institutional guidelines for the care and use of animals were followed. All procedures performed in studies involving animals were in accordance with the ethical standards and with the formal approval of the Animal Ethics Committee at the Universidad Andrés Bello institution.

Liver histopathology Liver sections from the right lobe of all mouse livers were routinely fixed in 10% formalin and embedded in paraffin. Hematoxylin and eosin was then carried out according to the standard procedures [15].

Biochemical determinations Serum alanine aminotransferase (ALT) was quantified using the Kovalent kit (Rio de Janeiro, Brazil) following manufacturer instructions, as described previously [15].

Contractile properties After treatment, the mice were anesthetized, the GA muscles were removed, and the muscle contractile properties were measured as previously described [47]. The maximum isometric tetanic force was determined. The muscle mass and the optimum muscle length (L_0) were used to calculate the specific net force [force normalized per total muscle fiber cross-sectional area (CSA), mN/mm^2] [13, 53, 54].

Weightlifting test At the end of the treatment, the mice were subjected to a measurement of muscle strength by a weightlifting test as previously described [25]. Briefly, the apparatus consisted of a series of chain links of increasing length attached to a ball of tangled fine wire. The number of links ranged from one to seven with total weights between 15.5 and 54.1 g. Before performing the test and prior to treatments, the mice were subjected to training (once per day for 2 weeks). To perform the test, the mouse grasps (with its forepaws) the different weights and a score was assigned. The final score was calculated as the summation of the product between the link weight and the time held. The average of three measures from each mouse was normalized by the body weight [47].

Running test Mice were subjected to perform exercises on a treadmill for 15 min at 20 cm/s on a treadmill, divided in three sessions of 5 min with a rest of 5 min. The test was recorded and the video analyzed to calculate the mice's permanence time in three zones of the treadmill, accordingly to scheme of Fig. 2a.

Rotarod test Before starting the experiment, the mice were accustomed to the rotarod for 1 week, at different rotation speeds in 5-min-long sessions. The rotarod test was performed before starting the treatment with normal or DDC diet, and also during weeks 1, 3, 4, 5, and 6 of the treatments. To perform the test, mice were placed in the rotarod, with an initial rotation speed of 5 rpm. The speed was gradually increased from 5 to 35 rpm over a time of 5 min. The time (in seconds) that mice spend on the rotarod was recorded.

Footprint test The footprint test was used to measure the gait of mice. To obtain footprints, the hind- and forefeet of the

mice were coated with non-toxic blue paint. The animals were then allowed to walk along a 38-cm-long, 5.2-cm-wide runway (with 5-cm-high walls) into an enclosed box. All mice had three training runs and were then given one run per week. A fresh sheet of white paper was placed on the floor of the runway for each run. The footprint patterns were analyzed for three step parameters (all measured in centimeters): (1) *stride length* was measured as the average distance of forward movement between each stride. (2) *Stance length* was measured as the average distance between left and right hind footprints, (3) *sway length* of the posterior base was measured as the average distance between the left and right hind footprints and left, and these values were determined by measuring the perpendicular distance of a given step to a line connecting its opposite preceding and proceeding steps. For each step parameter, three values were measured from each run, excluding footprints made at the beginning and end of the run where the animal was initiating and finishing movement, respectively. The mean value of each set of three values was used in subsequent analysis.

Locomotor activity test Spontaneous locomotor activity was measured in open-field chambers measuring 50 cm long, 30 cm wide, and 20 cm high, in a room with lighting and noise-free and was used to compare the mobility of mice fed with a normal (Control) or DDC diet for 6 weeks. The mice were placed in the arena and allowed to freely move for 5 min while recording with a camera above. The images are analyzed by a made-home automated tracking system. Traveled distance was calculated from the locomotor activity data. After each test session, the equipment was cleaned with 70% ethanol to remove animal odors.

Water and food intakes The animals were separated in individual cages 2 weeks previous to the start of the experiment and kept during the complete period of treatment using like a bed paper pelletized that allow major absorption of fluids. Food and water were weekly administered in fixed amounts (200 ml of water and 200 g of ground food), and the intakes were measured at 0, 3, and 6 weeks by difference between the remainder and the initial food and water for each mouse [4].

Muscle fiber's diameter determination and quantification Cryosections (7 μm) of the GA were stained with Alexa-Fluor® 594 tagged WGA (Life Technologies™, USA) according to standard procedures. Fiber sizes were determined by WGA staining and the Image J software (NIH, USA), as previously described [19, 50]. In brief, fibers were manually selected, and the minimal Feret diameter of each fiber was computed by the software. Myofiber cross-sectional area (CSA) was determined and measured regarding to the fiber types, as previously reported [49].

Determination of fiber types For determining of fiber types in the GA muscles, immunofluorescence analysis of MHC expression was performed with primary antibodies against the specific types of myosin [11]. For this, cryosections of GA were rinsed once with PBS, then incubated 30 min with mouse-to-mouse blocking reagent (1:100 in PBS), then incubated with a blocking solution (PBS, 10% goat serum, 1:100 mouse-to-mouse blocking reagent) for 1 h. After of this incubation, a mix of antibodies were used: MHC-I (BA-D5, 1:10), MHC-IIA (SC-71, 1:300), and MHC-IIB (BF-F3, 1:50), in blocking solution for 2 h. All the primary antibodies were purchased from the Developmental Studies Hybridoma Bank (University of Iowa). Then, the sections were rinsed three times for 5 min with PBS. A mix of secondary antibodies (Invitrogen, USA) were incubated for 1 h (1:250; Alexa IgG2b, A21140; Alexa IgM, A21426; Alexa IgG1, A21121). The slides were washed in PBS three times and were mounted with a fluorescent mounting medium (Dako Corporation, USA). Finally, the slides were visualized with a Motic BA310 fluorescence microscopy. Fiber types were determined within the entire muscle/cross-section (red, IIB; green, IIA; blue, I; black or no stained, IIX and mixed) and then counted. The quantification of fiber type was expressed as the percentages that were individually calculated in each image and further plotted.

Measurement of the ROS Fresh-frozen GA muscles were cryosectioned to 7 μm and placed on glass slides. The sections were washed twice with ice-cold HBSS (Hank's Balanced Salt Solution) and incubated with the cell permeate dye dichlorodihydrofluorescein (H2-DCF-DA) (5 μM , Invitrogen, USA) for 15–30 min in the dark at room temperature. Then, the sections were rinsed twice with HBSS and once PBS, and then were fixed with 4% paraformaldehyde for 10 min and rinsed with PBS. Further, cryosections were incubated with 1 $\mu\text{g}/\text{ml}$ Hoechst 33258 in PBS for 10 min for nuclear staining. After rinsing, the sections were mounted with fluorescent mounting medium (Dako Corporation, CA), viewed and photographed using the Motic BA310 epifluorescence microscope (Motic, Hong Kong) to 488 nm. Muscle sections were immediately analyzed and the ROS production was measured by the increases in DCF fluorescence, as an indicator of ROS production. The ROS levels were quantified by the analysis of DCF fluorescence intensity in the pictures using the software Image J [2].

Immunoblot analysis GA muscles were homogenized in Tris-EDTA buffer with a cocktail of protease inhibitors and 1 mM PMSF. Proteins were subjected to SDS-PAGE, transferred onto PDVF membranes (Millipore, USA), and probed with mouse anti-MHC (1:3000; MF-20, Developmental Studies, Hybridoma Bank, University of Iowa, USA), goat anti-4-hydroxynonenal (4HNE) (1:1000; Merck, USA), mouse

anti-atrogin-1 (1:500; Santa Cruz Biotechnology, USA), rabbit anti-MuRF-1 (1:500; Santa Cruz Biotechnology, USA), mouse anti-tubulin (1:5000; Santa Cruz Biotechnology, USA), and mouse anti- β -actin (Abcam, USA; 1:2000). All immunoreactions were visualized by enhanced chemiluminescence (Thermo Scientific, USA).

Determination of ubiquitinated MHC protein levels Total protein extracts were immuno-precipitated with mouse anti-MHC (1:100; MF-20, Developmental Studies, Hybridoma Bank, University of Iowa, USA). The antibody/antigen complex was then pulled out of the sample using protein G-coupled agarose beads to isolate MHC. The immuno-precipitated extract was separated in SDS-PAGE and transferred to PVDF membranes that were incubated with the antibodies for ubiquitin (1:1000; Santa Cruz Biotechnology, USA), MHC (1:3000; MF-20, Developmental Studies, Hybridoma Bank, University of Iowa, USA), and β -actin (1:5000; Merck, USA). All immunoreactions were visualized by enhanced chemiluminescence (Thermo Scientific, USA) that were acquired using the Fotodyne FOTO/Analyst Luminary Workstation Systems (Fotodyne, Inc., USA). Densitometry analysis was determined by scanning immunoreactive bands, and intensity values were obtained for further normalization against the control group.

Determination of carbonylated protein levels Carbonylation modification in GA muscle was assessed by immunoblot detection of protein carbonyl groups, using the OxyBlot assay following the indications of the supplier (OxyBlot Protein Oxidation Detection Kit, Millipore, S7150). Briefly, 30 μg of total proteins was subjected to SDS-PAGE and transferred to PVDF membranes, which were incubated with the antibodies provided in the kit. All immunoreactions were visualized by enhanced chemiluminescence (Thermo Scientific, USA), which were acquired using the Fotodyne FOTO/Analyst Luminary Workstation Systems (Fotodyne, Inc., USA). Densitometry analysis was determined by scanning immunoreactive bands, and intensity values were obtained for further normalization against the control group.

Quantitative real-time PCR analysis RNA was isolated from liver samples using the SV Total RNA Isolation System (Promega, Madison, WI) and then quantified spectrophotometrically in a NanoDrop ND-1000 (NanoDrop Technologies, Wilmington, DE). cDNA synthesis was performed starting with 1 μg of total RNA (Improm II system; Promega, Madison, WI) according to the manufacturer's guidelines. We measured the hepatic expression of Col1A1.

All probes were obtained from Applied Biosystems (Foster City, CA). The relative amounts of all mRNAs were calculated using the comparative threshold cycles (dCT) method and normalized to 18S RNA as a housekeeping gene.

Magnetic resonance imaging (MRI) protocol In vivo MR imaging was performed using a 1 T Bruker ICON MR scanner (Bruker, MA, USA). Briefly, anesthetized mice were imaged in the prone position. Following a 3D gradient echo scout scan, an ECG gated, T1-Flash cine images for cardiac function analysis were acquired (imaging parameters—FOV, 25×25 mm; matrix acquisition, $116 \times 116 \times 6$; in-plane resolution, 0.21×0.21 mm). Muscle quantification was performed from T1w abdominal MR (imaging parameters—FOV, 30×30 mm; matrix acquisition, $256 \times 256 \times 12$; in-plane resolution, 0.12×0.12 mm) [51].

MRI analysis Cardiac function was studied calculating the end-systolic and end-diastolic left ventricle volume and the ejection fraction using OsiriX (OsiriX Foundation, Geneva, Switzerland). Psoas muscle volume was calculated by manual segmentation in the T1w images using OsiriX.

Cell cultures The skeletal muscle cell line C₂C₁₂ obtained from the American Type Culture Collection was grown in DMEM 10% fetal bovine serum and differentiated into myotubes until day 5 with DMEM 2% horse serum [3].

Cell viability (MTT assays) Cytotoxicity was determined by the MTT assay. C₂C₁₂ myotubes were incubated with or without several concentrations of DDC (between 0 and 400 μ g/ml) in DMEM 2% horse serum for 24 h. At the end of experiment, 10 μ l of MTT solution (5 mg/ml, pH 7.5) was added. After 1 h, blue formazan crystals were resolved with 100 μ l of DMSO. Absorbance was measured at 595 nm. Cell viability (percent of control) was calculated relative to untreated control.

Atrophic effect in vitro C₂C₁₂ myotubes were incubated with DDC (10 or 25 μ g/ml) or serum from mice fed with control or DDC-supplemented diets (10% final) for 72 h. The MHC protein levels were determined by Western blot as previously described [19].

Statistics For statistical analysis, we used a *t* test to compare two groups. To compare three or more groups, we used one or two-way analysis of variance (ANOVA) with a post hoc Bonferroni multiple-comparison test (Prisma). A difference was considered statistically significant at $P < 0.05$.

Results

DDC-fed mice exhibit liver damage, muscle weakness and loss of muscle functionality

We evaluated the effects of chronic liver damage on strength and muscle function. For this purpose, hepatic injury was induced in mice by a diet supplemented with

DDC hepatotoxin for 6 weeks, a model in which there is considerable hepatic dysfunction evidenced by histological alterations in the third week (ESM-1A): increased liver weight (ESM-1B), ALT activity (ESM-1C), and Col1A1 expression (ESM-1D) [32].

Several functional tests with live mice were performed on chow and DDC-supplemented diet fed mice along 6 weeks. Figure 1a indicates mice with chronic liver damage caused by consuming the DDC diet experienced a decrease in their muscle's ability to support weight beginning in the second week after receiving the DDC diet when a weightlifting test was performed. At the end of the experiment (week 6), muscle strength fell until it reached 40% of the value obtained from the normal diet control group. Another functional test conducted was on exercise performance using the rotarod test. Figure 1b demonstrates that the riding time for the control mice fed with the normal diet remained unchanged during the 6 weeks of treatment. However, mice fed with the DDC diet showed a decline in the riding time beginning in the third week of treatment and reaching the minimal value at the end of the sixth week (25% of the control group).

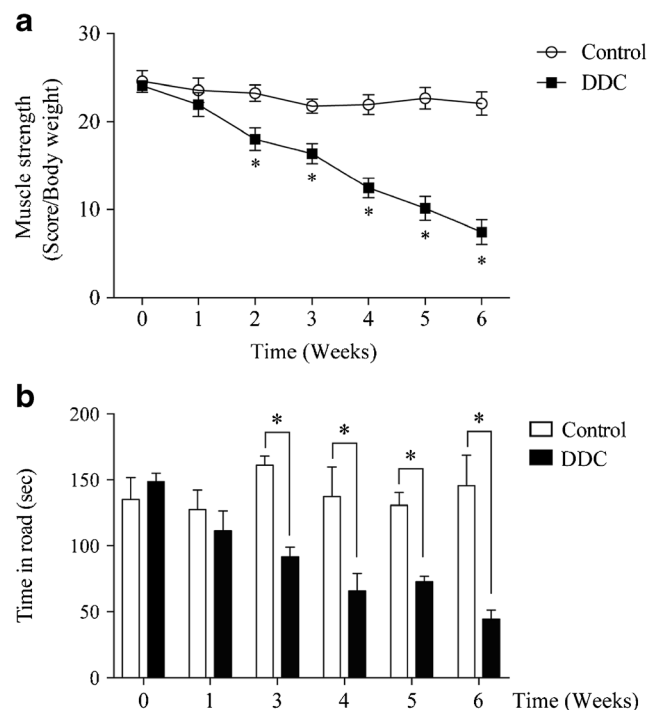


Fig. 1 Mice with chronic liver damage induced by a DDC-supplemented diet develop muscular weakness. C57BL/6J male mice were fed a standard chow (Control) or DDC-supplemented diet (DDC) for 6 weeks. Each week, mice were subjected to the following: **a** A weightlifting test to determine limb muscle strength. Values represent the score normalized per body weight reached by the mice with each weight and correspond to the mean \pm SEM (five animals per group, three independent experiments; * $P < 0.05$ vs. Control, two-way ANOVA). **b** A rotarod test. The values correspond to the time (s). The values correspond to the mean \pm SEM (five animals per group, three independent experiments; * $P < 0.05$ vs. Control, two-way ANOVA)

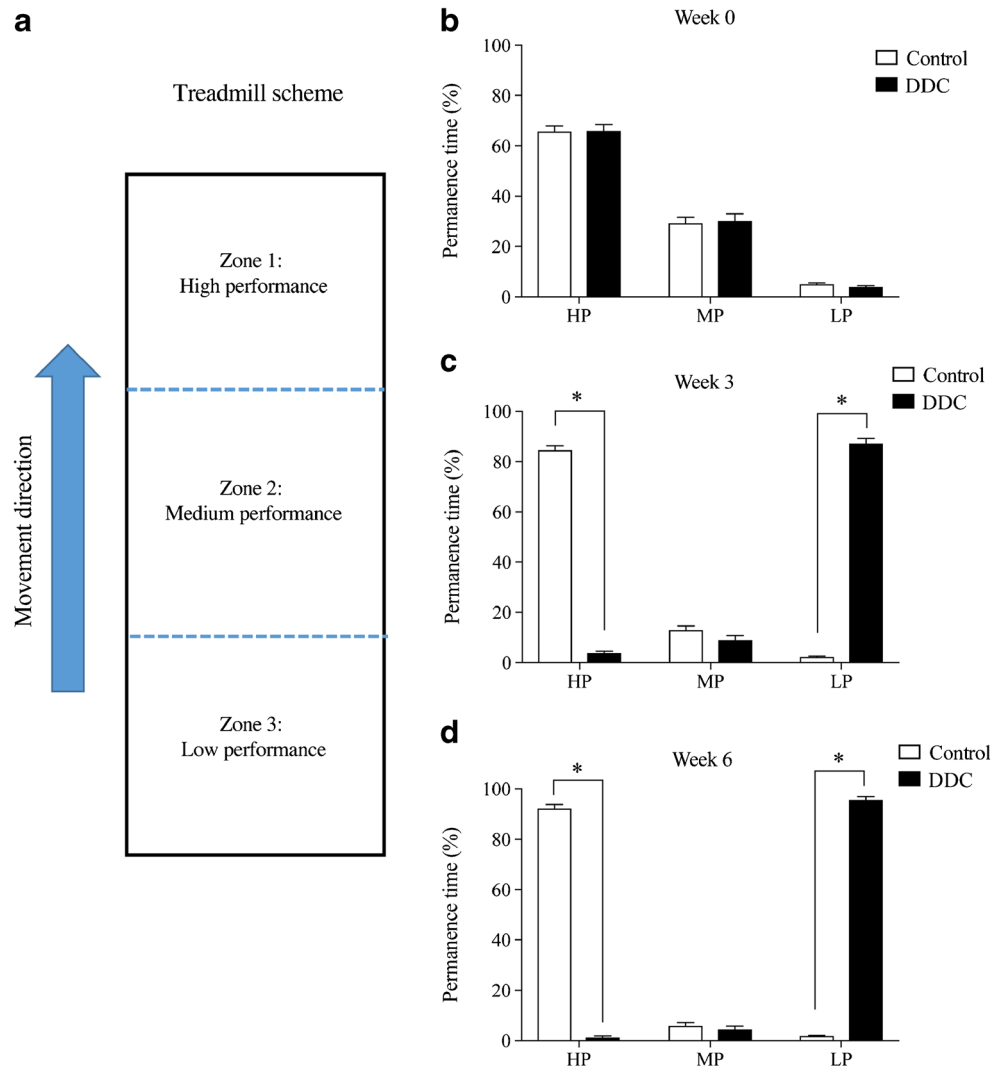
Then we evaluated exercise performance on a treadmill by measuring how much time mice spent running over the front, middle, or bottom of treadmill's sections. These measures were categorized as follows: front section was categorized as high performance (HP), the middle section was referred to as medium performance (MP), and the last portion was categorized as low performance (LP), as displayed in Fig. 2a. The results indicate at the beginning of the experiment (week 0), both groups of mice (Control or DDC) have a similar permanence time in treadmill's distinct zones, with a higher proportion in the HP (Fig. 2b). However, after 3 weeks of treatment, mice fed the DDC diet spent a shorter length of time in the HP zone (3.86 vs. 84.6% of control mice) and more time in the LP zone (87.2 vs. 2.3% of control mice), indicating an impairment in physical performance (Fig. 2c). This situation was accentuated in the sixth week after treatment where mice fed the DDC diet only reached 1.5% of permanence time in the HP zone (control mice 92.3%), while they spent 94.1% of permanence time in LP zone (control mice 1.8%) (Fig. 2d).

Thus, these results reveal CLD that caused by the DDC diet impaired exercise performance in mice.

To determine whether the changes observed in the functional tests for living mice can be extrapolated to a specific deficiency in skeletal muscle, we evaluated the muscle strength in isolated gastrocnemius tissue through electrophysiological assays of tetanic force. Figure 3a reflects muscles from mice fed the DDC diet had a lower muscle force in most of the assessed frequency ranges. Figure 3b shows gastrocnemius from mice fed the DDC diet presented a decrease in maximal tetanic force (381 mN/mm²) compared to the control group (548 mN/mm²). Similar results were obtained by evaluating the maximal tetanic force in the tibialis anterior muscle (ESM-2).

To rule out the possibility that mice fed the DDC diet had a problem with the motricity of their paws, we conducted a footprint test. ESM-3A displays the scheme of this test and the distances measured. Results presented in ESM-3B, C, and D suggest there were no differences between mice fed the

Fig. 2 Chronic liver damage induced by DDC-supplemented diet impairs the ability to perform physical exercise. **a** Treadmill scheme in which is illustrated the treadmill and the three zones used to calculate exercise performance: high (HP), medium (MP), and low (LP) performance zones of the treadmill. Each experiment was recorded by video and further analyzed for the permanence time in each zone. Briefly, C57BL/6J male mice were trained to run on a treadmill before the beginning of the experiment with a standard chow (Control) or DDC-supplemented diet (DDC) for 6 weeks. In weeks 0 (**b**), 3 (**c**), and 6 (**d**) after the mice were fed the differential diet, mice were subjected to the running test to measure exercise performance. The permanence time (s) was calculated from observing video footage and expressed as the percentage of time spent in each of the three zones. The values correspond to the mean \pm SEM (five animals per group, three independent experiments; * $P < 0.05$ vs. Control, two-way ANOVA)



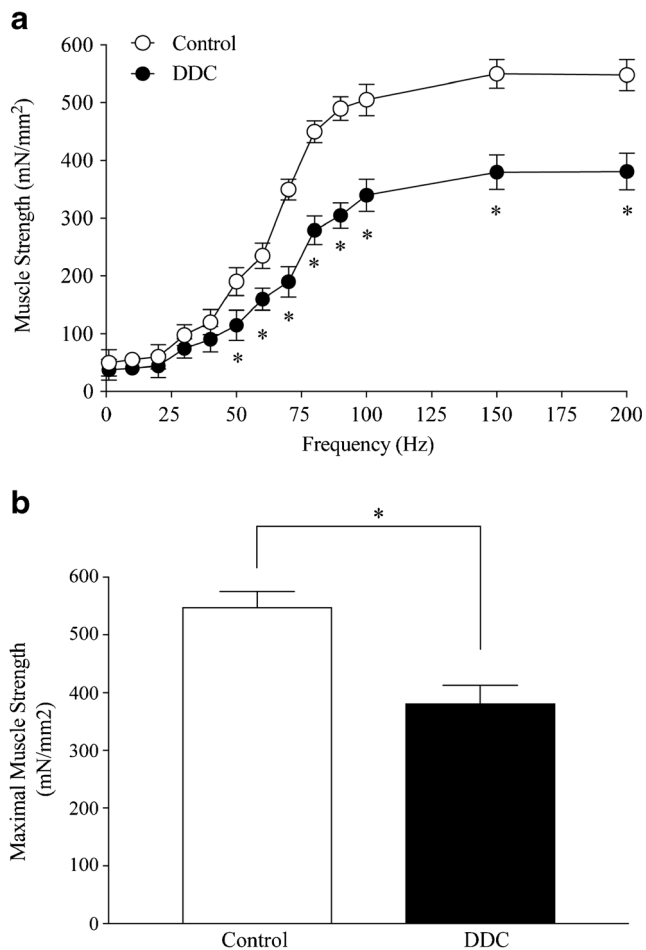


Fig. 3 Gastrocnemius (GA) tissue from mice with chronic liver disease has decreased isometric force. C57BL/6J male mice were fed a standard chow (Control) or DDC-supplemented diet (DDC) for 6 weeks. At the end of the experiment, GA muscles were excised. **a** A curve of force versus frequency was determined ($*P < 0.05$ vs. Control, two-way ANOVA). **b** Maximal isometric strength (mN/mm²) was evaluated. Values represent the mean \pm SEM of three independent experiments. In each experiment, five mice were used for each experimental condition ($*P < 0.05$ vs. Control, *t* test)

control or DDC diet in the stride, stance, and sway length of their hind paws, respectively, suggesting motor skills were not altered in mice fed the DDC diet. Additionally, we evaluated the locomotor activity of mice using an open field test. Tracings of the distance walked by mice fed either the normal (ESM-4A) or DDC diet (ESM-4B). Quantification of this data determines the mobility of both experimental groups is similar (ESM-4C).

We also evaluated several other parameters such as body weight, muscle mass, and food and water intake. Figure 4a demonstrates mice fed the DDC diet experienced a decline in body weight evidenced in the third and sixth weeks of treatment, reaching 17.1 g compared to the control group's 26.8 g in the sixth week. Mice from the DDC group indicated the ratio between the mass of gastrocnemius tissue and body weight was lower (5.1) than the control group's (5.9) at the

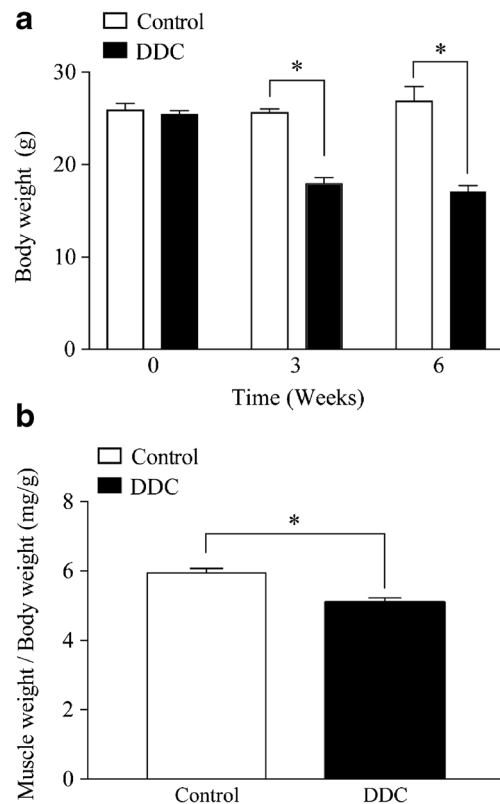


Fig. 4 Mice with chronic liver disease have a decreased body and gastrocnemius (GA) weight. **a** C57BL/6J male mice were fed a standard chow (Control) or DDC-supplemented diet (DDC) for 6 weeks. **a** At 0, 3, and 6 weeks, body weight was measured. The value is expressed in grams. Values represent the mean \pm SEM of three independent experiments. In each experiment, five mice were used for each experimental condition ($*P < 0.05$ vs. Control, two-way ANOVA). **b** At the end of experiment (week 6), GA tissue weight was measured. The values represent the ratio between GA tissue and body weight (mg/g) and are the mean \pm SEM of three independent experiments. In each experiment, five mice were used for each experimental condition. ($*P < 0.05$ vs. Control, *t* test)

end of the experiment (Fig. 4b). Interestingly, mice from the control and DDC groups did not have differences among them or at the time of treatment regarding food and water intake (ESM-5A and B, respectively).

Overall, these results suggest chronic liver damage induced by the intake of a DDC-supplemented diet produced muscle weakness evidenced by decreased exercise performance and isometric tetanic force which would not be explained by changes in motor skills, immobility, or food or water intake.

Mice fed the DDC diet have a decrease in the myofiber diameter of gastrocnemius (GA) muscles

To evaluate the diameter of muscle fibers, a WGA stain was performed on GA muscle. Figure 5a shows GA tissue from mice fed the DDC diet showed a decrease in muscle fiber diameter. Quantification of the Feret's diameter revealed GA tissue from the control group has a normal distribution curve

with a peak in the range of 41–45 μm , whereas the fibers' size distribution from mice fed the DDC diet was clearly displaced to the left and experienced a peak in the range of 31–35 μm , indicating a smaller diameter than the control group (Fig. 5b). These data suggest GA tissue from mice fed the DDC diet has a decrease in myofiber diameter. To evaluate muscle atrophy in another muscle, we measured the volume of psoas by MRI analysis. Our data showed that mice fed with DDC for 3 weeks present a decrease in the volume of psoas compared to control mice (EMS-6A). Interestingly, the cardiac function evaluated by MRI analysis was unchanged between mice fed with control and DDC diet (EMS-6B).

Gastrocnemius (GA) from mice with chronic liver damage presents transition in the fiber type

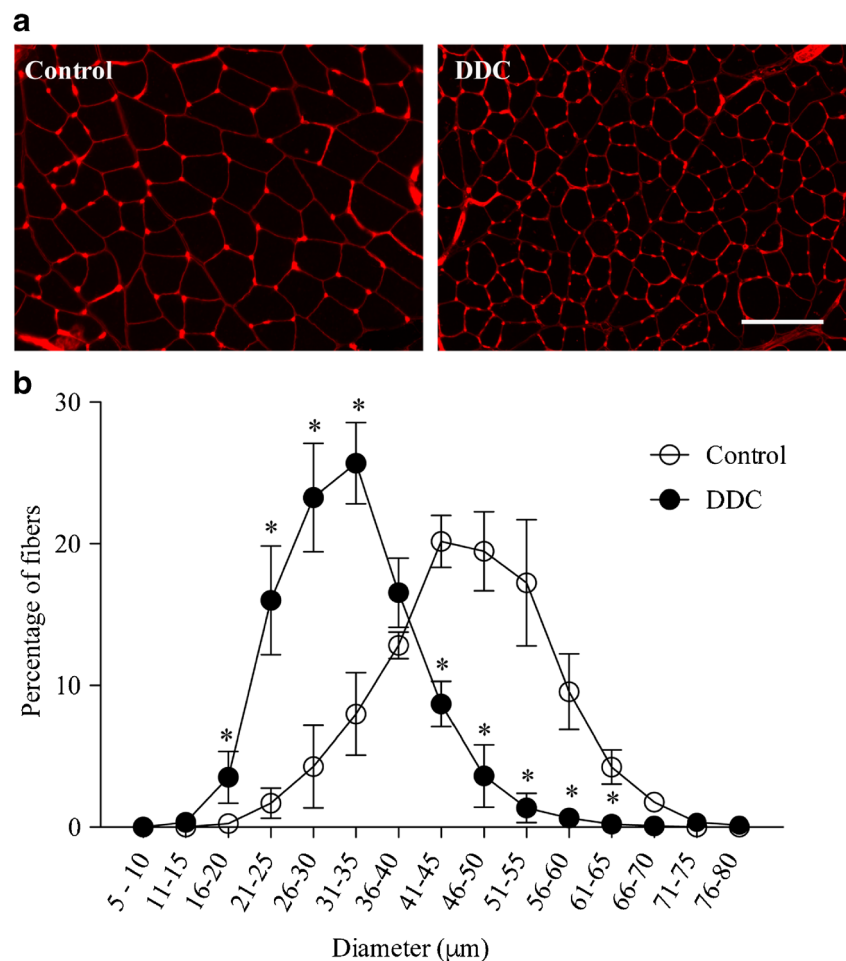
The most abundant fiber type in GA tissue is IIB [1]. When atrophied, there is a transition from IIB fibers to IIA and I fibers as well as hybrid fibers IIB/IIX, IIX, IIX/IIA (Fig. 6a) [38, 57]. In mice fed the DDC-supplemented diet, GA tissue exhibits a clear decrease in IIB fibers (from 63% in control mice to 27% in DDC mice) also as an increase in IIX (from 9% in control mice to 14% in DDC mice) and IIA fibers (from

13% in control mice to 29% in DDC mice) (Fig. 6b). The same also reflects there is an increase in the number of type I fibers (from 0% in control mice to 10% in DDC mice). In addition, we evaluated the CSA of the different fibers' types. GA from mice fed with DDC diet show a decrease of CSA in IIB and IIX fibers, and an increase in IIA fibers compared to mice fed with control diet (Fig. 6c). Normally, in GA, the CSA of IIB is bigger than IIA, so this transition in the fiber types (IIB to IIA) could explain the displacement of fiber diameter toward minor size (Fig. 5b). Our results suggest that in this case it is not the reason because CSA of IIA is increased in mice fed with DDC diet. However, since GA in normal conditions is a muscle that is mainly composed for IIB fibers, the decrease in its proportion and CSA can explain the displacement of fiber diameter toward minor size (Fig. 5b).

Gastrocnemius (GA) tissue from mice with chronic liver damage has decreased myosin heavy chain protein levels but higher levels of ubiquitination than control mice

One of the main targets altered in skeletal muscle atrophy is the sarcomeric proteins, specifically MHC. Therefore, we

Fig. 5 Gastrocnemius (GA) tissue from mice with chronic liver disease have decreased fiber diameters. C57BL/6J male mice were fed a standard chow (Control) or DDC-supplemented diet (DDC) for 6 weeks. At the end of the experiment, GA muscles were excised. **a** Muscle cross-sections were stained with WGA to delimit muscle fiber sarcolemma. **b** Minimal Feret diameters were determined in TA cross-sections from experiments depicted in (a). Fiber diameters were grouped from 0 to 80 μm and values expressed as the percentage of the total fibers quantified. Counted images are representative of three independent experiments, using five mice for each experimental condition. Values correspond to the mean \pm SEM. (* $P < 0.05$ vs. Control, two-way ANOVA)



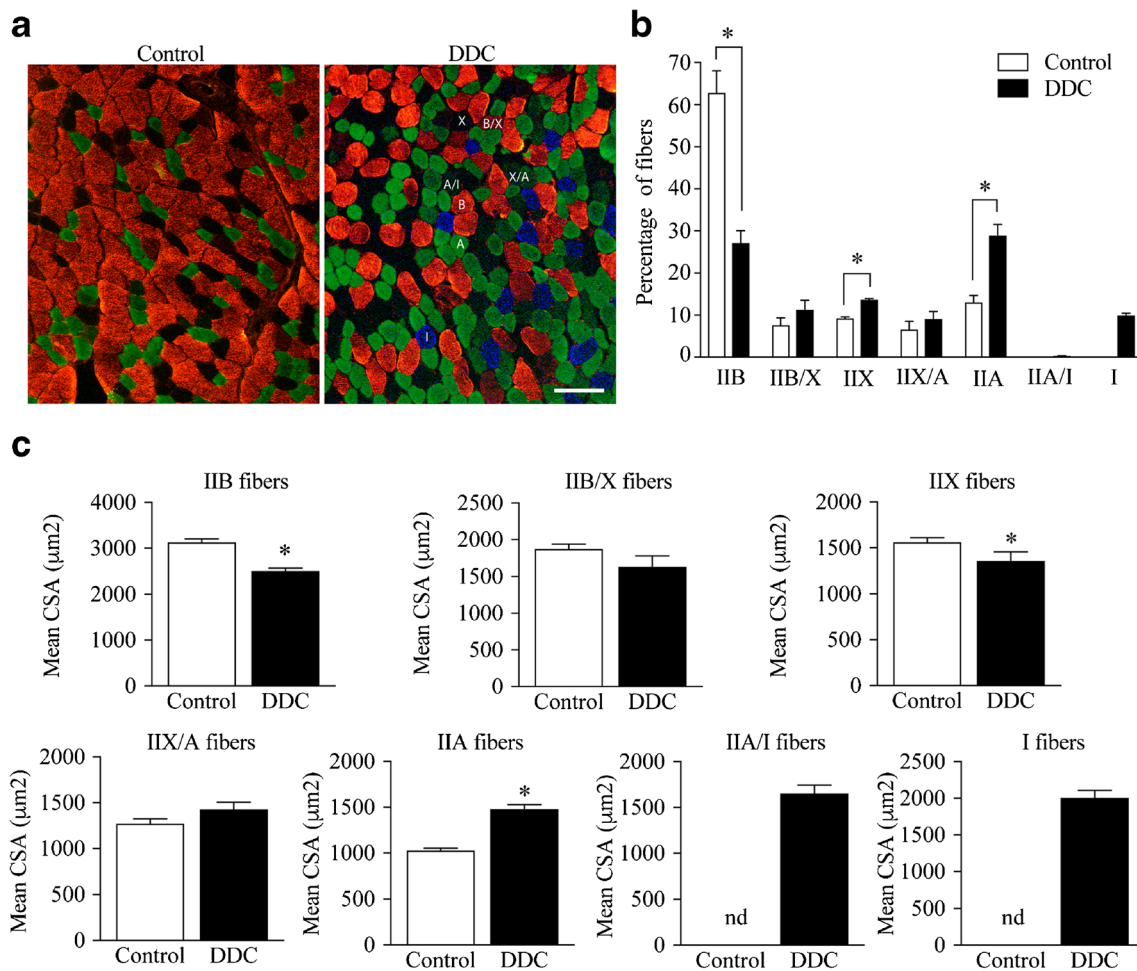


Fig. 6 Mice with chronic liver damage induced by DDC-supplemented diet have fiber type transitions in the gastrocnemius (GA) muscle. C57BL/6J male mice were fed a standard chow (Control) or DDC-supplemented diet (DDC) for 6 weeks. **a** At the end of the experiment, mice were sacrificed, and the GA muscles were analyzed to determine fiber type through the immunofluorescence detection of myosin heavy chain isoforms (IIA, IIB, I). Images obtained at $\times 40$ magnification reveal fiber types were determined within the entire muscle/cross-section (red, IIB; green, IIA; blue, I; black or not stained, IIX; and mixed, IIB/X, X/IIA, IIA/I). **b** Quantitative analysis of the fiber type. Graph representing

the percentage of specific fiber types relative to the total fibers counted per field. Values represent the mean \pm SEM of three independent experiments. In each experiment, five mice were used for each experimental condition ($*P < 0.05$ vs. Control, two-way ANOVA). **c** Analysis of CSA for each type of fiber. Images from GA obtained in the experiments for (a) were used for the quantitative analysis. Values represent the mean \pm SEM (μm^2) of three independent experiments. In each experiment, five mice were used for each experimental condition ($*P < 0.05$ vs. Control, *t* test)

evaluated MHC levels using a Western blot analysis. Figure 7a demonstrates the decrease in MHC protein levels in GA tissue from mice fed the DDC diet compared to the control group. This decline is 0.58-fold compared to control group (Fig. 7b).

The main pathway involved in altered MHC protein levels is the UPS, which ubiquitinates MHC before its degradation. To evaluate this, MHC was immunoprecipitated with an MHC antibody and then immunodetected with ubiquitin antibody using the Western blot method. Figure 7c shows GA tissue's total MHC protein levels decreased in mice from the DDC group as presented in Fig. 7a, but MHC ubiquitination levels are 2.4-fold higher in GA tissue from mice fed the DDC diet compared to the control diet (Fig. 7c, d).

Skeletal muscle from mice with chronic liver disease exhibits an increase of MuRF-1 and atrogin-1 expression

To assess the UPS's involvement, we evaluated the protein levels of atrogin-1 and MuRF-1, two key enzymes involved in the process of skeletal muscle atrophy. Figure 8a and c illustrates GA muscles from mice fed the DDC diet had increases in both atrogin-1 and MuRF-1. These increases are 2.0-fold for atrogin-1 and 4.4-fold for MuRF-1, compared to the control group's GA tissue (Fig. 8b and d, respectively).

These results suggest GA tissue from mice with CLD has a UPS more active to degrade muscle proteins than control mice.

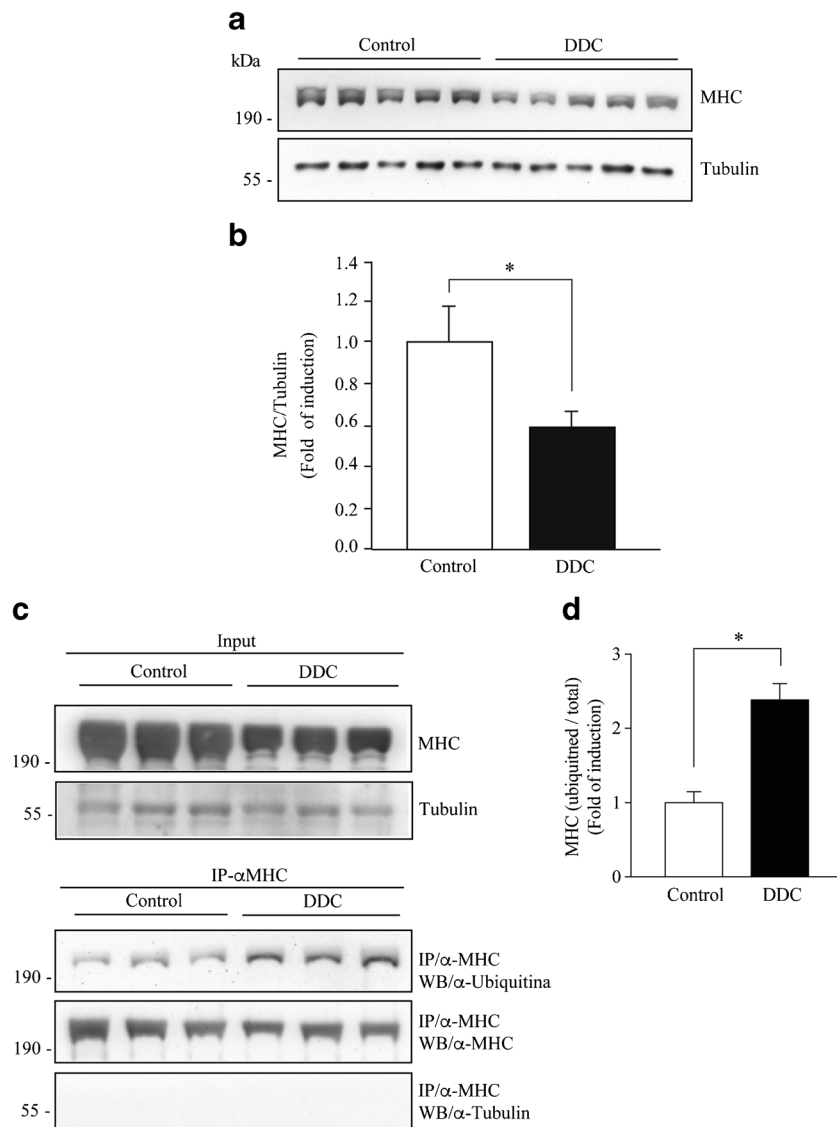


Fig. 7 Mice with chronic liver damage induced by DDC-supplemented diet have decreased myosin heavy chain (MHC) protein levels in the gastrocnemius (GA) muscle. C57BL/6J male mice were fed a standard chow (Control) or DDC-supplemented diet (DDC) for 6 weeks. At the end of the experiment, mice were sacrificed, and the GA muscles were excised and homogenized to evaluate **a** MHC protein levels through Western blot analysis. Tubulin levels were used as the loading control. Molecular weight markers are depicted in kilodaltons. **b** Quantitative analysis of the experiments from (a). Values represent the mean \pm SEM of three independent experiments. In each experiment, five mice were used for each experimental condition ($*P < 0.05$ vs. Control, *t* test). **c**

Ubiquitinated-MHC protein levels through immunoprecipitation with anti-MHC and further Western blot with anti-ubiquitin. The upper panel illustrates the immunodetection of MHC and tubulin in the input. The lower panel shows the detection of ubiquitinated-MHC levels in the immunoprecipitated. Tubulin is depicted as a negative control. Molecular weight markers are shown in kilodaltons. **d** Quantitative analysis of the experiments from (c). The levels of ubiquitinated MHC were normalized to total MHC and expressed relative to control. Values represent the mean \pm SEM of three independent experiments. In each experiment, five mice were used for each experimental condition ($*P < 0.05$ vs. Control, *t* test)

Gastrocnemius (GA) tissue from mice with chronic liver damage presents oxidative stress

To assess the involvement of oxidative stress, we evaluated the ROS levels in a slice of GA muscle. A DCF probe was used to detect and quantify ROS (Fig. 9a). The GA tissue of mice fed the DDC diet presented a higher ROS reactivity (an 8.3-fold increase compared to mice fed the control diet) (Fig. 9b). We subsequently evaluated consequences of

oxidative stress by protein modifications such as carbonylation and 4-HNE. Figure 9c and d show GA tissue from mice fed the DDC diet has higher levels of carbonylated proteins than mice fed the normal diet (2.2-fold vs. control mice). Moreover, Fig. 9e and f reflects that GA tissue from the DDC group has greater 4-HNE reactivity compared to the control group (2.0-fold vs. control mice).

All these results suggest GA tissue from mice with CLD developed oxidative stress.

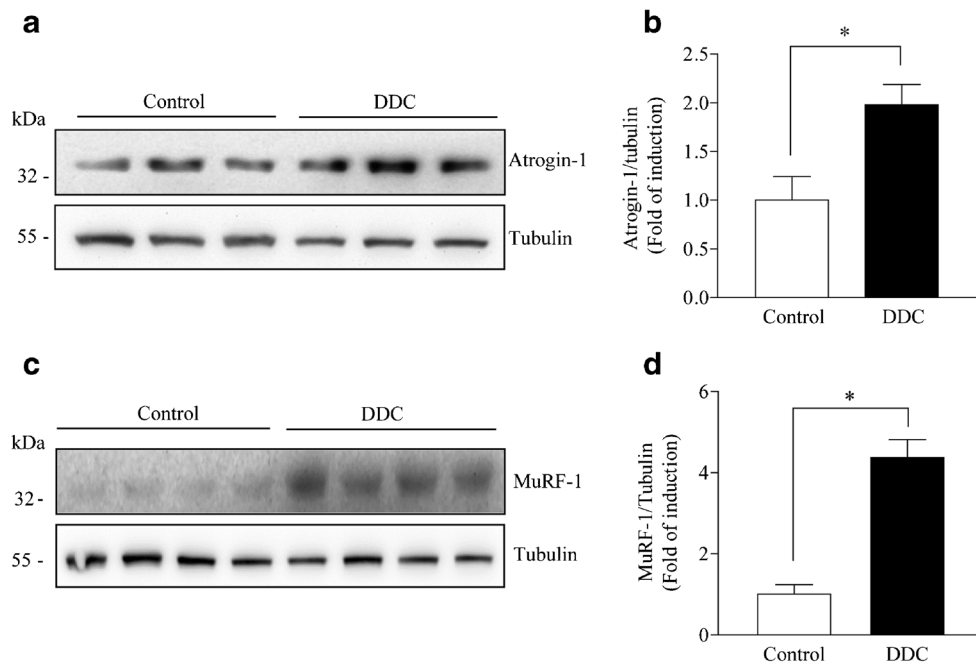


Fig. 8 Gastrocnemius (GA) tissue from mice with chronic liver disease develop increased atrogin-1 and MuRF-1 protein levels. C57BL/6J male mice were treated with standard chow (Control) or DDC-supplemented diet (DDC) for 6 weeks. At the end of the treatment, mice were sacrificed, and the GA muscles were excised and homogenized to evaluate of atrogin-1 (a) and MuRF-1 (c) protein levels by Western blot. Tubulin

levels were used as the loading control. Molecular weight markers are shown in kilodaltons. Quantitative analysis of the atrogin-1 (b) and MuRF-1 (d). Values represent the mean \pm SEM of three independent experiments. In each experiment, five mice were used for each experimental condition (* $P < 0.05$ vs. Control, t test)

Hepatotoxin DDC did not directly induce an atrophic effect in skeletal muscle cells

A possible explanation for the atrophic effect observed in GA is that DDC directly affect skeletal muscle. To evaluate this, we incubated C₂C₁₂ myotubes with different concentrations of DDC. First, we determined that myotubes maintained the viability between 1 and 50 μ g/ml of DDC and decreased in 100, 200, and 400 μ g/ml of DDC (EMS-7A). In the same figure, it can be observed that serum from mice fed with DDC diet, but not with control diet, decreased the MHC levels. Interestingly, DDC increased the HO-1 expression in C₂C₁₂ myotubes (EMS-7B), an effect that has been reported in other cell types [56]. The same figure shows that serum from mice fed with control or DDC diet did not change the HO-1 expression from basal levels.

Further, we evaluated the effect of DDC and serum from mice fed with DDC on the MHC protein levels. Thus, myotubes incubated with 1 and 50 μ g/ml of DDC did not present changes in the MHC protein levels (Fig. 10a, b).

These results suggest that DDC did not directly induce an atrophic effect in skeletal muscle cells, and that there is a soluble factor in the serum from mice fed with DDC that induces skeletal muscle atrophy.

Discussion

In this paper, we demonstrated that a murine model of CLD induced by the DDC hepatotoxin showed an evident muscular weakness with decreased fiber diameter and MHC total protein levels. Among the mechanisms involved in this atrophic effect, we demonstrated that UPS is overactivated by detecting increased levels of ubiquitinated MHC, atrogin-1, and MuRF-1, and we demonstrated important evidence of oxidative stress by the increased ROS as well as carbonylated- and 4-HNE-modified protein levels.

This model of CLD [32, 46] has not been previously characterized for muscular weakness. To address this gap in the research literature, several approaches with live mice were performed in which the DDC group always exhibited lower muscular strength or performance than control mice, which is consistent with clinical observations in patients with CLD [21, 40, 52, 59]. Furthermore, these results agree with data regarding isometric and tetanic force measured in isolated gastrocnemius tissue, in which the DDC group exhibited decreased muscle strength.

Among the factors associated with mortality in patients with CLD are poor physical fitness and endurance [27]. Regarding these factors, we observed that basal mobility was unchanged by the DDC diet, while mice in the DDC group demonstrated lesser ability to perform an involuntary

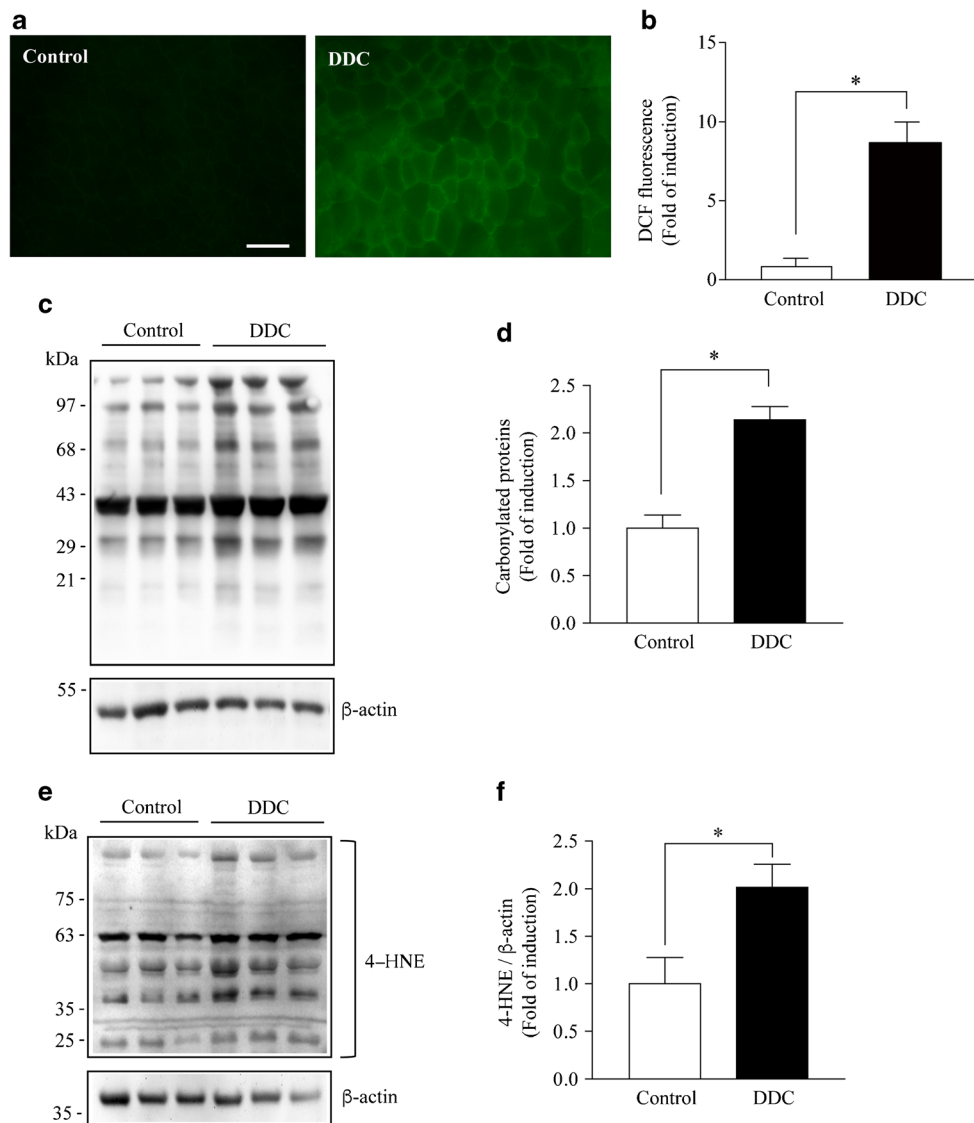


Fig. 9 Gastrocnemius (GA) tissue from mice with chronic liver disease has an increase of ROS and protein oxidation levels. C57BL/6J male mice were treated with standard chow (Control) or DDC-supplemented diet (DDC) for 6 weeks. At the end of the treatment, mice were sacrificed, and the GA muscles were excised. **a** Cryosections obtained from the GA tissue were incubated with a DCF probe for ROS detection through fluorescence microscopy. **b** Quantification of ROS levels from experiments demonstrated in (a). The values are expressed as the fold of induction of the DCF probe intensity ($*P < 0.05$ vs. Control, *t* test). **c** Levels of oxidation-dependent carbonylated protein levels were detected by Western blot using Oxyblot kit. β-Actin levels were used as the

loading control. Molecular weight markers are shown in kilodaltons. **d** Quantitative analysis based in the densitometry of the bands. Values represent the mean \pm SEM of three independent experiments. In each experiment, five mice were used for each experimental condition ($*P < 0.05$ vs. Control, *t* test). **e** Levels of oxidation-dependent 4HNE protein adducts were detected by Western blot using anti-4HNE antibody. β-Actin levels were used as the loading control. Molecular weight markers are shown in kilodaltons. **f** Quantitative analysis based in the densitometry of the bands. Values represent the mean \pm SEM of three independent experiments. In each experiment, five mice were used for each experimental condition ($*P < 0.05$ vs. Control, *t* test)

exercise test on a treadmill. Similar results were obtained with the rotarod test. Interestingly, our data suggest that in the DDC model of CLD, immobilization does not contribute to muscle weakness. Thus, our data reveal there were no significant differences in mobility or motor skills test scores between the experimental and control groups, allowing us to assert immobility or motor problems did not cause the observed muscle weakness. The measures of water and food intake were not significantly different between the control and DDC mice,

suggesting caloric and liquid intake did not cause the DDC mice's decreased body and muscle weight. Despite these data, we must acknowledge nutrient absorption problems could impact body and muscle weight.

In addition, our results suggest that the muscle wasting can be observed in mice at early stages after DDC treatment (from 2 to 3 weeks in different muscles, e.g., gastrocnemius, tibialis anterior, and psoas). In our hands, DDC treatment did not show change in the cardiac function at early stages, despite

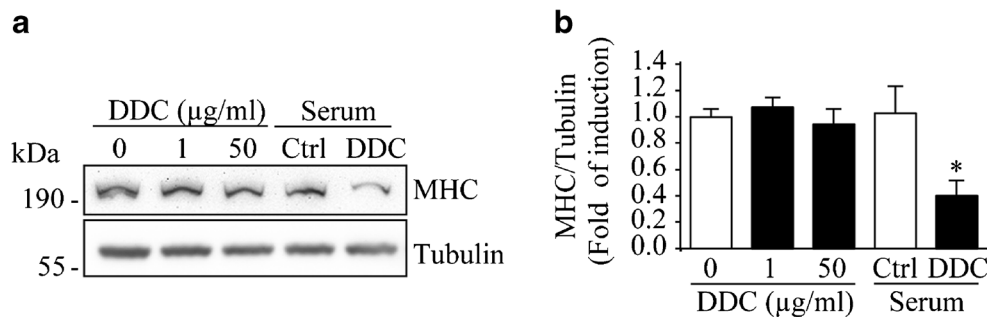


Fig. 10 Serum from mice fed with DDC-supplemented diet contain a factor, different to DDC itself, produces muscle atrophy in vitro. C_2C_{12} myoblasts were differentiated into myotubes for 5 days. **a** Myotubes were incubated with DDC (1 and 50 $\mu\text{g/ml}$) or serum derived from mice fed with control (Serum Ctrl) or DDC diet (Serum DDC) at the final concentration of 10% v/v. After of 72 h of incubation, MHC levels were

determined by Western blot analysis. Tubulin levels were used as a loading control. Molecular weights are indicated in kilodaltons. **b** Quantitative analysis for MHC levels was conducted, with values normalized to tubulin levels and plotted as fold of induction relative to control (* $P < 0.05$ vs. Control, one-way ANOVA)

it has been previously reported [26] which can be explained by the different experimental approaches to measure the cardiac parameters. Moreover, we cannot discard that alterations of cardiac function induced by DDC later stages could contribute to muscle function in alive mice. In this line, the diminution in isometric muscle strength in isolated muscle is a parameter which is independent of cardiac function.

Our data indicate that DDC-treated mice have lesser muscle strength than control, which was evident when mice were subjected to an exercise challenge. Patients with cirrhosis also exhibit decreased physical activity [77]. However, most of these patients also present other comorbidities that affect the physical activity like obesity [70] which is absent in our model. Thus, other experiments must be done in order to evaluate the contribution of those factors in the physical activity of cirrhotic patients or experimental models of CLD.

Regarding mechanisms involved in muscle atrophy, we evaluated the involvement of UPS and oxidative stress. Our data confirm muscle-specific E3 ligases MuRF-1 and atrogin-1 are increased in DDC mice. Moreover, these data are consistent with the decreased levels of total MHC and increased levels of ubiquitinated MHC, a step prior to degrading MHC by proteasome. Thus, we can suggest the decrease in MHC levels caused by CLD can be explained, at least, for an increase in its ubiquitination by MuRF-1 which is increased in muscle tissue from mice fed the DDC diet. Moreover, we detected an increase in ROS levels which could be responsible for the increase in MuRF-1 levels. Thus, we can speculate that in CLD, skeletal muscle increments ROS production concomitantly with the MuRF-1 expression and the ubiquitination and degradation of MHC. However, it is not possible to disregard the involvement of a synthesis mechanism which could be decreased in CLD. Previously, we have demonstrated that ROS can induce the increase of the E3 ubiquitin-ligases MuRF-1 and atrogin-1, which can be avoided by N-acetylcysteine (NAC) treatment [2]. NAC is an antioxidant agent widely used to reduce ROS content and oxidative stress.

Thus, in further studies, NAC treatment could be a useful tool to elucidate if oxidative stress is responsible for MuRF-1 and atrogin-1 expression induction.

Interestingly, our evidence suggests there is oxidative stress in the skeletal muscle DDC-fed mice. In addition to the ROS increase, we detected an increment of the protein modifications dependent on oxidative stress such as 4-HNE and carbonylation [5, 42]. These findings are relevant because they not only detected an early event such as ROS increases but also determined the oxidative stress-induced cellular damage by the modification of proteins, which could not be the only result of cell damage because it has been DNA and cell membranes can be also be altered [62, 68]. Regarding the carbonylation of protein, there is evidence that in several models of muscle atrophy such as disuse, aging, or sarcopenia in cancer, sepsis, or COPD, there is an increase of carbonylated proteins dependent on oxidative stress [5, 61]. Several studies have demonstrated carbonylation and most posttranslational oxidative modifications may result in loss of protein function as well as accelerated protein degradation by the proteasome [17, 20, 31, 48, 58].

Myofibrillar proteins such as actin and myosin are among the main targets [30]. Thus, further experiments must be performed to study possible MHC carbonylation and the effect on its degradation by proteasome in muscles from mice with CLD. In other models of muscle wasting such as disuse muscle atrophy, oxidative stress may contribute to the muscle dysfunction by the increment of protein catabolism through activation of calpains, caspase-3, and UPS [60]. Oxidative stress can trigger the activation of calpains responsible for myofilament disassembly as well as caspase-3, which can degrade actin and MHC [60, 61].

Another underlying mechanism have to be involved regarding skeletal muscle atrophy induction since food intake and mobility were not affected in DDC-fed mice. In this line, it is plausible to think that unknown molecules can be released from the liver into the blood, reaching the muscles and acting

endocrine. In this context, when the liver is damaged, there are inflammatory processes that are activated and several soluble molecules can be released into the blood [75, 76], events that have been also shown in mice fed with DDC diet [32, 33]. These molecules can reach the muscle by the circulation. Interestingly, some of these factors, such as tumor necrosis factor alpha (TNF- α) [9, 72, 80] and interleukin-6 (IL-6) [7, 35, 55], have been described as muscle wasting inducers in other types of chronic diseases. Indeed, CLD can develop a condition denominated hyperammonemia, which is characterized by an increase in the ammonia concentration in the blood due to a disruption in the urea cycle [24]. This ammonia increment can damage other organs, mainly the brain [41]. Recent studies have also involved this condition with muscle wasting in patients with cirrhosis [23]. The muscle expresses ammonia transporters [73], and growing evidence have shown that ammonia could induce the transcription of myostatin in the skeletal muscle [64], a protein widely described as an atrophic factor in the skeletal muscle [39, 65].

Another CLD feature that could be involved in the skeletal muscle atrophy is the increment of bile acids in the blood circulation. Bile acids have been described as a signaling molecule and metabolism modulator in peripheral tissues [18, 45, 79]. In this line, recent studies in patients with non-alcoholic fatty liver disease (NAFLD) have linked to this condition with changes in the muscle volume [43].

Finally, another possible explanation for the atrophic effect observed in skeletal muscle after DDC treatment is that DDC itself can directly produce muscle wasting. The way that DDC can reach the skeletal muscle is by the blood circulation. However, there are no reports regarding DDC pharmacokinetics after diet uptake. Our *in vitro* results indicated that serum from mice fed with DDC did not contain an amount of DDC able to increase HO-1 expression (or simply is absent of the serum), an effect that has been previously described to be directly induced by DDC [56]. Interestingly, we determined that serum from DDC-treated mice induced muscle atrophy *in vitro* whereas DDC *per se* did not, reinforcing the idea that the serum contains an unknown soluble factor, different to DDC itself, able to induce muscle wasting.

In this paper, we described some mechanisms involved in muscle wasting produced in a murine model of chronic liver disease. Our study could suggest the use of antioxidants or proteasome inhibitors to decrease the causes of muscle atrophy and weakness such as oxidative stress or UPS activity.

Acknowledgements This study was supported by research grants from the National Fund for Science & Technology Development [FONDECYT 1161646 (C.C.V.), 1161288 (F.S.); 11171001 (D.C.); 1150327 (M.A.)], Millennium Institute on Immunology and Immunotherapy [P09-016-F (F.S.)]; Programa de Cooperación Científica ECOS-CONICYT [C16S02 (C.C.V.)]; Center for Aging and Regeneration [CARE PFB12/2007 (M.A.)]; Fondecip EQM [150033 (M.E.A.)]; UNAB-DI [741-15/N (C.C.V., F.S.)]. J.A. thanks Conicyt for providing a PhD Scholarship

(21161353). F.C. thanks Universidad Andrés Bello-Dirección de Investigación for providing a PhD Scholarship.

Author's contribution J.A., F.C., F.A., and B.G. were responsible for carrying out the experiments as well as analyzing and interpreting the data. D.C., S.K., and M.A. were responsible for collecting and reporting liver-related data. MEA was responsible for carrying out the MRI analysis. C.C.V. and F.S. were involved in drafting the manuscript for publication. C.C.V. was responsible for conceiving all the experiments and was involved in analyzing the data, preparing it for publication, and drafting the manuscript.

Compliance with ethical standards

Conflict of interest The authors declare that they have no conflict of interest.

References

1. Abrigo J, Rivera JC, Aravena J, Cabrera D, Simon F, Ezquer F, Ezquer M, Cabello-Verrugio C (2016) High fat diet-induced skeletal muscle wasting is decreased by mesenchymal stem cells administration: implications on oxidative stress, ubiquitin proteasome pathway activation, and myonuclear apoptosis. *Oxidative Med Cell Longev* 2016:9047821–9047813. <https://doi.org/10.1155/2016/9047821>
2. Abrigo J, Rivera JC, Simon F, Cabrera D, Cabello-Verrugio C (2016) Transforming growth factor type beta (TGF- β) requires reactive oxygen species to induce skeletal muscle atrophy. *Cell Signal* 28:366–376. <https://doi.org/10.1016/j.cellsig.2016.01.010>
3. Abrigo J, Simon F, Cabrera D, Cabello-Verrugio C (2016) Angiotensin-(1-7) prevents skeletal muscle atrophy induced by transforming growth factor type beta (TGF- β) via mas receptor activation. *Cell Physiol Biochem* 40:27–38. <https://doi.org/10.1159/000452522>
4. Bachmanov AA, Reed DR, Beauchamp GK, Tordoff MG (2002) Food intake, water intake, and drinking spout side preference of 28 mouse strains. *Behav Genet* 32:435–443
5. Barreiro E (2016) Role of protein carbonylation in skeletal muscle mass loss associated with chronic conditions. *Proteomes* 4. <https://doi.org/10.3390/proteomes4020018>
6. Barrera F, Zuniga P, Arrese M (2015) Prediction of esophageal variceal bleeding in liver cirrhosis: is there a role for hemostatic factors? *Semin Thromb Hemost* 41:481–487. <https://doi.org/10.1055/s-0035-1550438>
7. Belizario JE, Fontes-Oliveira CC, Borges JP, Kashiabara JA, Vannier E (2016) Skeletal muscle wasting and renewal: a pivotal role of myokine IL-6. *Springerplus* 5:619. <https://doi.org/10.1186/s40064-016-2197-2>
8. Berzigotti A, Seijo S, Reverter E, Bosch J (2013) Assessing portal hypertension in liver diseases. *Expert Rev Gastroenterol Hepatol* 7: 141–155. <https://doi.org/10.1586/egh.12.83>
9. Bhatnagar S, Panguluri SK, Gupta SK, Dahiya S, Lundy RF, Kumar A (2010) Tumor necrosis factor- α regulates distinct molecular pathways and gene networks in cultured skeletal muscle cells. *PLoS One* 5:e13262. <https://doi.org/10.1371/journal.pone.0013262>
10. Bilodeau PA, Coyne ES, Wing SS (2016) The ubiquitin proteasome system in atrophying skeletal muscle: roles and regulation. *Am J Physiol Cell Physiol* 311:C392–C403. <https://doi.org/10.1152/ajpcell.00125.2016>

11. Bloemberg D, Quadrilatero J (2012) Rapid determination of myosin heavy chain expression in rat, mouse, and human skeletal muscle using multicolor immunofluorescence analysis. *PLoS One* 7: e35273. <https://doi.org/10.1371/journal.pone.0035273>
12. Bonaldo P, Sandri M (2013) Cellular and molecular mechanisms of muscle atrophy. *Dis Model Mech* 6:25–39. <https://doi.org/10.1242/dmm.010389>
13. Cabello-Verrugio C, Morales MG, Cabrera D, Vio CP, Brandan E (2012) Angiotensin II receptor type 1 blockade decreases CTGF/CCN2-mediated damage and fibrosis in normal and dystrophic skeletal muscles. *J Cell Mol Med* 16:752–764. <https://doi.org/10.1111/j.1582-4934.2011.01354.x>
14. Cabello-Verrugio C, Rivera JC, Garcia D (2017) Skeletal muscle wasting: new role of nonclassical renin–angiotensin system. *Curr Opin Clin Nutr Metab Care* 20:158–163. <https://doi.org/10.1097/MCO.0000000000000361>
15. Cabrera D, Ruiz A, Cabello-Verrugio C, Brandan E, Estrada L, Pizarro M, Solis N, Torres J, Barrera F, Arrese M (2016) Diet-induced nonalcoholic fatty liver disease is associated with sarcopenia and decreased serum insulin-like growth Factor-1. *Dig Dis Sci* 61:3190–3198. <https://doi.org/10.1007/s10620-016-4285-0>
16. Carey EJ, Lai JC, Wang CW, Dasarathy S, Lobach I, Montano-Loza AJ, Dunn MA, Fitness LE, Exercise in Liver Transplantation C (2017) A multicenter study to define sarcopenia in patients with end-stage liver disease. *Liver Transpl* 23:625–633. <https://doi.org/10.1002/lt.24750>
17. Chacon-Cabrera A, Mateu-Jimenez M, Langohr K, Fermoselle C, Garcia-Arumi E, Andreu AL, Yelamos J, Barreiro E (2017) Role of PARP activity in lung cancer-induced cachexia: effects on muscle oxidative stress, proteolysis, anabolic markers, and phenotype. *J Cell Physiol* 232:3744–3761. <https://doi.org/10.1002/jcp.25851>
18. Chiang JY (2013) Bile acid metabolism and signaling. *Compr Physiol* 3:1191–1212. <https://doi.org/10.1002/cphy.c120023>
19. Cisternas F, Morales MG, Meneses C, Simon F, Brandan E, Abrigo J, Vazquez Y, Cabello-Verrugio C (2015) Angiotensin-(1–7) decreases skeletal muscle atrophy induced by angiotensin II through a mas receptor-dependent mechanism. *Clin Sci (Lond)* 128:307–319. <https://doi.org/10.1042/CS20140215>
20. Cunha TF, Bacurau AV, Moreira JB, Paixao NA, Campos JC, Ferreira JC, Leal ML, Negrao CE, Moriscot AS, Wisloff U, Brum PC (2012) Exercise training prevents oxidative stress and ubiquitin-proteasome system overactivity and reverse skeletal muscle atrophy in heart failure. *PLoS One* 7:e41701. <https://doi.org/10.1371/journal.pone.0041701>
21. Dasarathy S (2012) Consilience in sarcopenia of cirrhosis. *J Cachexia Sarcopenia Muscle* 3:225–237. <https://doi.org/10.1007/s13539-012-0069-3>
22. Dasarathy S (2014) Treatment to improve nutrition and functional capacity evaluation in liver transplant candidates. *Curr Treat Options Gastroenterol* 12:242–255. <https://doi.org/10.1007/s11938-014-0016-9>
23. Dasarathy S (2017) Myostatin and beyond in cirrhosis: all roads lead to sarcopenia. *J Cachexia Sarcopenia Muscle* 8:864–869. <https://doi.org/10.1002/jcsm.12262>
24. Dasarathy S, Hatzoglou M (2018) Hyperammonemia and proteostasis in cirrhosis. *Curr Opin Clin Nutr Metab Care* 21:30–36. <https://doi.org/10.1097/MCO.0000000000000426>
25. Deacon RM (2013) Measuring the strength of mice. *J Vis Exp*. <https://doi.org/10.3791/2610>
26. Desai MS, Shabier Z, Taylor M, Lam F, Thevananther S, Kusters A, Karpen SJ (2010) Hypertrophic cardiomyopathy and dysregulation of cardiac energetics in a mouse model of biliary fibrosis. *Hepatology* 51:2097–2107. <https://doi.org/10.1002/hep.23585>
27. Duarte-Rojo A, Ruiz-Margain A, Montano-Loza AJ, Macias-Rodriguez R, Ferrando A, Kim WR (2017) Exercise and physical activity for patients with ESLD: improving functional status and sarcopenia while on the transplant waitlist. *Liver Transpl* 24:122–139. <https://doi.org/10.1002/lt.24958>
28. Durand F, Valla D (2008) Assessment of prognosis of cirrhosis. *Semin Liver Dis* 28:110–122. <https://doi.org/10.1055/s-2008-1040325>
29. Ebner N, Steinbeck L, Doehner W, Anker SD, von Haehling S (2014) Highlights from the 7th Cachexia conference: muscle wasting pathophysiological detection and novel treatment strategies. *J Cachexia Sarcopenia Muscle* 5:27–34. <https://doi.org/10.1007/s13539-014-0136-z>
30. Fedorova M, Kuleva N, Hoffmann R (2009) Reversible and irreversible modifications of skeletal muscle proteins in a rat model of acute oxidative stress. *Biochim Biophys Acta* 1792:1185–1193. <https://doi.org/10.1016/j.bbadis.2009.09.011>
31. Fermoselle C, Rabinovich R, Ausin P, Puig-Vilanova E, Coronell C, Sanchez F, Roca J, Gea J, Barreiro E (2012) Does oxidative stress modulate limb muscle atrophy in severe COPD patients? *Eur Respir J* 40:851–862. <https://doi.org/10.1183/09031936.00137211>
32. Fickert P, Stoger U, Fuchsbichler A, Moustafa T, Marschall HU, Weiglein AH, Tsybrovskyy O, Jaeschke H, Zatloukal K, Denk H, Trauner M (2007) A new xenobiotic-induced mouse model of sclerosing cholangitis and biliary fibrosis. *Am J Pathol* 171:525–536. <https://doi.org/10.2353/ajpath.2007.061133>
33. Fickert P, Thueringer A, Moustafa T, Silbert D, Gumhold J, Tsybrovskyy O, Lebofsky M, Jaeschke H, Denk H, Trauner M (2010) The role of osteopontin and tumor necrosis factor alpha receptor-1 in xenobiotic-induced cholangitis and biliary fibrosis in mice. *Lab Invest* 90:844–852. <https://doi.org/10.1038/labinvest.2010.61>
34. Gabrielli M, Vivanco M, Hepp J, Martinez J, Perez R, Guerra J, Arrese M, Figueroa E, Soza A, Yanes R, Humeres R, Rios H, Palacios JM, Zapata R, Sanhueza E, Contreras J, Rencoret G, Rossi R, Jarufe N (2010) Liver transplantation results for hepatocellular carcinoma in Chile. *Transplant Proc* 42:299–301. <https://doi.org/10.1016/j.transproceed.2009.11.034>
35. Haddad F, Zaldivar F, Cooper DM (1985) Adams GR (2005) IL-6-induced skeletal muscle atrophy. *J Appl Physiol* 98:911–917. <https://doi.org/10.1152/jappphysiol.01026.2004>
36. Hansen J, Brandt C, Nielsen AR, Hojman P, Whitham M, Febbraio MA, Pedersen BK, Plomgaard P (2011) Exercise induces a marked increase in plasma follistatin: evidence that follistatin is a contraction-induced hepatokine. *Endocrinology* 152:164–171. <https://doi.org/10.1210/en.2010-0868>
37. Hasselgren PO, Menconi MJ, Fareed MU, Yang H, Wei W, Evenson A (2005) Novel aspects on the regulation of muscle wasting in sepsis. *Int J Biochem Cell Biol* 37:2156–2168. <https://doi.org/10.1016/j.biocel.2005.01.017>
38. Higashino K, Matsuura T, Sukanuma K, Yukata K, Nishisho T, Yasui N (2013) Early changes in muscle atrophy and muscle fiber type conversion after spinal cord transection and peripheral nerve transection in rats. *J Neuroeng Rehabil* 10:46. <https://doi.org/10.1186/1743-0003-10-46>
39. Huang Z, Chen X, Chen D (2011) Myostatin: a novel insight into its role in metabolism, signal pathways, and expression regulation. *Cell Signal* 23:1441–1446. <https://doi.org/10.1016/j.cellsig.2011.05.003>
40. Imai K, Takai K, Watanabe S, Hanai T, Suetsugu A, Shiraki M, Shimizu M (2017) Sarcopenia impairs prognosis of patients with hepatocellular carcinoma: the role of liver functional reserve and tumor-related factors in loss of skeletal muscle volume. *Nutrients* 9. <https://doi.org/10.3390/nu9101054>
41. Khan A, Ayub M, Khan WM (2016) Hyperammonemia is associated with increasing severity of both liver cirrhosis and hepatic encephalopathy. *Int J Hepatol* 2016:6741754–6741755. <https://doi.org/10.1155/2016/6741754>

42. Kim Y, Men SS, Liang C, Receno CN, Brutsaert TD, Korol DL, Heffernan KS, DeRuisseau KC (2017) Effects of long-term exposures to low iron and branched-chain amino acid containing diets on aging skeletal muscle of fisher 344 Brown Norway rats. *Appl Physiol Nutr Metab* 43:165–173. <https://doi.org/10.1139/apnm-2017-0272>
43. Kobayashi Y, Hara N, Sugimoto R, Mifuji-Moroka R, Tanaka H, Eguchi A, Iwasa M, Hasegawa H, Iwata K, Takei Y, Taguchi O (2017) The associations between circulating bile acids and the muscle volume in patients with non-alcoholic fatty liver disease (NAFLD). *Intern Med* 56:755–762. <https://doi.org/10.2169/internalmedicine.56.7796>
44. Lazaridis KN, LaRusso NF (2015) The cholangiopathies. *Mayo Clin Proc* 90:791–800. <https://doi.org/10.1016/j.mayocp.2015.03.017>
45. Li T, Chiang JY (2015) Bile acids as metabolic regulators. *Curr Opin Gastroenterol* 31:159–165. <https://doi.org/10.1097/MOG.000000000000156>
46. Liedtke C, Luedde T, Sauerbruch T, Scholten D, Stretz K, Tacke F, Tolba R, Trautwein C, Trebicka J, Weiskirchen R (2013) Experimental liver fibrosis research: update on animal models, legal issues and translational aspects. *Fibrogenesis Tissue Repair* 6:19. <https://doi.org/10.1186/1755-1536-6-19>
47. Marquez-Miranda V, Abrigo J, Rivera JC, Araya-Duran I, Aravena J, Simon F, Pacheco N, Gonzalez-Nilo FD, Cabello-Verrugio C (2017) The complex of PAMAM-OH dendrimer with angiotensin (1–7) prevented the disuse-induced skeletal muscle atrophy in mice. *Int J Nanomedicine* 12:1985–1999. <https://doi.org/10.2147/IJN.S125521>
48. Mastrocola R, Reffo P, Penna F, Tomasinelli CE, Boccuzzi G, Baccino FM, Aragno M, Costelli P (2008) Muscle wasting in diabetic and in tumor-bearing rats: role of oxidative stress. *Free Radic Biol Med* 44:584–593. <https://doi.org/10.1016/j.freeradbiomed.2007.10.047>
49. McClung JM, Kavazis AN, DeRuisseau KC, Falk DJ, Deering MA, Lee Y, Sugiura T, Powers SK (2007) Caspase-3 regulation of diaphragm myonuclear domain during mechanical ventilation-induced atrophy. *Am J Respir Crit Care Med* 175:150–159. <https://doi.org/10.1164/rccm.200601-1420C>
50. Meneses C, Morales MG, Abrigo J, Simon F, Brandan E, Cabello-Verrugio C (2015) The angiotensin-(1–7)/mas axis reduces myonuclear apoptosis during recovery from angiotensin II-induced skeletal muscle atrophy in mice. *Pflugers Arch* 467:1975–1984. <https://doi.org/10.1007/s00424-014-1617-9>
51. Miras AD, Seyfried F, Phinikaridou A, Andia ME, Christakis I, Spector AC, Botnar RM, le Roux CW (2014) Rats fed diets with different energy contribution from fat do not differ in adiposity. *Obes Facts* 7:302–310. <https://doi.org/10.1159/000368622>
52. Montano-Loza AJ, Meza-Junco J, Prado CM, Lieffers JR, Baracos VE, Bain VG, Sawyer MB (2012) Muscle wasting is associated with mortality in patients with cirrhosis. *Clin Gastroenterol Hepatol* 10:166–173, 173 e161. <https://doi.org/10.1016/j.cgh.2011.08.028>
53. Morales MG, Cabello-Verrugio C, Santander C, Cabrera D, Goldschmeding R, Brandan E (2011) CTGF/CCN-2 over-expression can directly induce features of skeletal muscle dystrophy. *J Pathol* 225:490–501. <https://doi.org/10.1002/path.2952>
54. Morales MG, Cabrera D, Cespedes C, Vio CP, Vazquez Y, Brandan E, Cabello-Verrugio C (2013) Inhibition of the angiotensin-converting enzyme decreases skeletal muscle fibrosis in dystrophic mice by a diminution in the expression and activity of connective tissue growth factor (CTGF/CCN-2). *Cell Tissue Res* 353:173–187. <https://doi.org/10.1007/s00441-013-1642-6>
55. Munoz-Canoves P, Scheele C, Pedersen BK, Serrano AL (2013) Interleukin-6 myokine signaling in skeletal muscle: a double-edged sword? *FEBS J* 280:4131–4148. <https://doi.org/10.1111/febs.12338>
56. Nikam A, Patankar JV, Lackner C, Schock E, Kratky D, Zatloukal K, Abuja PM (2013) Transition between acute and chronic hepatotoxicity in mice is associated with impaired energy metabolism and induction of mitochondrial heme oxygenase-1. *PLoS One* 8:e66094. <https://doi.org/10.1371/journal.pone.0066094>
57. Pette D, Staron RS (2000) Myosin isoforms, muscle fiber types, and transitions. *Microsc Res Tech* 50:500–509. [https://doi.org/10.1002/1097-0029\(20000915\)50:6<500::AID-JEMT7>3.0.CO;2-7](https://doi.org/10.1002/1097-0029(20000915)50:6<500::AID-JEMT7>3.0.CO;2-7)
58. Pomies P, Blaquiére M, Maury J, Mercier J, Gouzi F, Hayot M (2016) Involvement of the FoxO1/MuRF1/Atrogin-1 signaling pathway in the oxidative stress-induced atrophy of cultured chronic obstructive pulmonary disease myotubes. *PLoS One* 11:e0160092. <https://doi.org/10.1371/journal.pone.0160092>
59. Ponziani FR, Gasbarrini A (2017) Sarcopenia in patients with advanced liver disease. *Curr Protein Pept Sci* 19:681–691. <https://doi.org/10.2174/1389203718666170428121647>
60. Powers SK, Duarte J, Kavazis AN, Talbert EE (2010) Reactive oxygen species are signalling molecules for skeletal muscle adaptation. *Exp Physiol* 95:1–9. <https://doi.org/10.1113/expphysiol.2009.050526>
61. Powers SK, Kavazis AN, DeRuisseau KC (2005) Mechanisms of disuse muscle atrophy: role of oxidative stress. *Am J Physiol Regul Integr Comp Physiol* 288:R337–R344. <https://doi.org/10.1152/ajpregu.00469.2004>
62. Powers SK, Kavazis AN, McClung JM (2007) Oxidative stress and disuse muscle atrophy. *J Appl Physiol* 102:2389–2397. <https://doi.org/10.1152/jappphysiol.01202.2006>
63. Powers SK, Morton AB, Ahn B, Smuder AJ (2016) Redox control of skeletal muscle atrophy. *Free Radic Biol Med* 98:208–217. <https://doi.org/10.1016/j.freeradbiomed.2016.02.021>
64. Qiu J, Thapaliya S, Runkana A, Yang Y, Tsien C, Mohan ML, Narayanan A, Egtesad B, Mozdziaik PE, McDonald C, Stark GR, Welle S, Naga Prasad SV, Dasarathy S (2013) Hyperammonemia in cirrhosis induces transcriptional regulation of myostatin by an NF-kappaB-mediated mechanism. *Proc Natl Acad Sci U S A* 110:18162–18167. <https://doi.org/10.1073/pnas.1317049110>
65. Qiu J, Tsien C, Thapalaya S, Narayanan A, Weihl CC, Ching JK, Egtesad B, Singh K, Fu X, DUBYAK G, McDonald C, Almasan A, Hazen SL, Naga Prasad SV, Dasarathy S (2012) Hyperammonemia-mediated autophagy in skeletal muscle contributes to sarcopenia of cirrhosis. *Am J Physiol Endocrinol Metab* 303:E983–E993. <https://doi.org/10.1152/ajpendo.00183.2012>
66. Rom O, Kaisari S, Reznick AZ, Aizenbud D (2014) Peroxynitrite induces degradation of myosin heavy chain via p38 MAPK and muscle-specific E3 ubiquitin ligases in C2 skeletal myotubes. *Adv Exp Med Biol* 832:1–8. https://doi.org/10.1007/5584_2014_9
67. Rom O, Reznick AZ (2016) The role of E3 ubiquitin-ligases MuRF-1 and MAFbx in loss of skeletal muscle mass. *Free Radic Biol Med* 98:218–230. <https://doi.org/10.1016/j.freeradbiomed.2015.12.031>
68. Rossi P, Marzani B, Giardina S, Negro M, Marzatico F (2008) Human skeletal muscle aging and the oxidative system: cellular events. *Curr Aging Sci* 1:182–191
69. Scicchitano BM, Pelosi L, Sica G, Musaro A (2017) The physiopathologic role of oxidative stress in skeletal muscle. *Mech Ageing Dev* 170:37–44. <https://doi.org/10.1016/j.mad.2017.08.009>
70. Shiraki M, Nishiguchi S, Saito M, Fukuzawa Y, Mizuta T, Kaibori M, Hanai T, Nishimura K, Shimizu M, Tsurumi H, Moriwaki H (2013) Nutritional status and quality of life in current patients with liver cirrhosis as assessed in 2007–2011. *Hepatol Res* 43:106–112. <https://doi.org/10.1111/hepr.12004>
71. Sinclair M, Gow PJ, Grossmann M, Angus PW (2016) Review article: sarcopenia in cirrhosis—etiology, implications and

- potential therapeutic interventions. *Aliment Pharmacol Ther* 43: 765–777. <https://doi.org/10.1111/apt.13549>
72. Spate U, Schulze PC (2004) Proinflammatory cytokines and skeletal muscle. *Curr Opin Clin Nutr Metab Care* 7:265–269
 73. Takeda K, Takemasa T (2015) Expression of ammonia transporters Rhbg and Rhcg in mouse skeletal muscle and the effect of 6-week training on these proteins. *Physiol Rep* 3. <https://doi.org/10.14814/phy2.12596>
 74. Tandon P, Ney M, Irwin I, Ma MM, Gramlich L, Bain VG, Esfandiari N, Baracos V, Montano-Loza AJ, Myers RP (2012) Severe muscle depletion in patients on the liver transplant wait list: its prevalence and independent prognostic value. *Liver Transpl* 18: 1209–1216. <https://doi.org/10.1002/lt.23495>
 75. Tilg H (2001) Cytokines and liver diseases. *Can J Gastroenterol* 15: 661–668
 76. Tilg H, Wilmer A, Vogel W, Herold M, Nolchen B, Judmaier G, Huber C (1992) Serum levels of cytokines in chronic liver diseases. *Gastroenterology* 103:264–274
 77. Toshikuni N, Arisawa T, Tsutsumi M (2014) Nutrition and exercise in the management of liver cirrhosis. *World J Gastroenterol* 20: 7286–7297. <https://doi.org/10.3748/wjg.v20.i23.7286>
 78. Wang CW, Feng S, Covinsky KE, Hayssen H, Zhou LQ, Yeh BM, Lai JC (2016) A comparison of muscle function, mass, and quality in liver transplant candidates: results from the functional assessment in liver transplantation study. *Transplantation* 100:1692–1698. <https://doi.org/10.1097/TP.0000000000001232>
 79. Watanabe M, Houten SM, Matak C, Christoffolete MA, Kim BW, Sato H, Messaddeq N, Harney JW, Ezaki O, Kodama T, Schoonjans K, Bianco AC, Auwerx J (2006) Bile acids induce energy expenditure by promoting intracellular thyroid hormone activation. *Nature* 439:484–489. <https://doi.org/10.1038/nature04330>
 80. Zhou J, Liu B, Liang C, Li Y, Song YH (2016) Cytokine signaling in skeletal muscle wasting. *Trends Endocrinol Metab* 27:335–347. <https://doi.org/10.1016/j.tem.2016.03.002>